

Nuclear breakup of Borromean nuclei

G. F. Bertsch and K. Hencken*

Institute for Nuclear Theory, University of Washington, Seattle, Washington 98195

H. Esbensen

Physics Division, Argonne National Laboratory, Argonne, Illinois 60439

(Received 1 August 1997)

We study the eikonal model for the nuclear-induced breakup of Borromean nuclei, using ^{11}Li and ^6He as examples. The full eikonal model is difficult to realize because of six-dimensional integrals, but a number of simplifying approximations are found to be accurate. The integrated diffractive and one-nucleon stripping cross sections are rather insensitive to the neutron-neutron correlation, but the two-nucleon stripping does show some dependence on the correlation. The distribution of excitation energy in the neutron-core final state in one-neutron stripping reactions is quite sensitive to the shell structure of the halo wave function. Experimental data favor models with comparable amounts of s and p waves in the ^{11}Li halo. [S0556-2813(98)03503-1]

PACS number(s): 25.60.Gc, 25.70.Mn, 21.45.+v, 27.20.+n

I. INTRODUCTION

Halo nuclei having a very weakly bound neutron pair (often referred to as Borromean nuclei) are interesting objects, but they are difficult to study experimentally. Secondary interactions in radioactive beams have been an important tool, with Coulomb excitation providing quantitative data about the excitation properties [1,2]. Nuclear excitation is also important from an experimental point of view, but the theoretical interpretation of nuclear reaction cross sections deserves closer attention. In this work we attempt to make a link, as quantitative as possible, between the nuclear excitation observables and the fundamental properties of a Borromean nucleus. The fact that correlations can play an important role makes this goal more difficult than for a nucleus with a single-nucleon halo. On the experimental side, we have been inspired by the work on ^{11}Li carried out at Ganil, NSCL, RIKEN and most recently at GSI. The extremely large Coulomb breakup cross section shows the halo character of the nucleus, but the details of its wave function have been controversial. Starting from the shell model, two of us [3] constructed a wave function that fits many Coulomb excitation measurements [4]. It had a dominant $p_{1/2}^2$ shell configuration, as one expects from Hartree-Fock theory. However, several measurements (see, for example, Ref. [5]) and also the spectroscopy of the nearby nucleus ^{11}Be suggest a leading $s_{1/2}^2$ configuration in ^{11}Li .

In principle, a nuclear-induced breakup gives independent information and so it is desirable to calculate the various cross sections and compare with experiment. A recent experiment [6] was carried out on a ^{12}C target at 280 MeV/nucleon. At that energy it is justified to treat the target-projectile interaction in the sudden approximation, using the NN forward scattering amplitude for the interaction. Thus we may neglect the evolution of the wave function

during the interaction time, provided we take the interaction from nucleon-nucleon scattering. The energy domain around 250 MeV has an additional advantage from a theoretical point of view: The real part of the NN forward-scattering amplitude goes through zero in this vicinity, so only the absorptive part of the interaction needs to be treated in the theory.

The nuclear excitation of Borromean nuclei have been considered by a number of authors [7–14]. In treating the differential cross sections, it is common to make a number of simplifying assumptions. We list them here.

(i) *Ground state wave function.* Neutron-neutron correlations were neglected in Ref. [8]. We shall apply wave functions that have the full three-particle correlations. It turns out that differential cross sections are quite insensitive to these correlations, except the two-neutron stripping, which does show an effect. Independent-particle models can only describe pure configurations, so a mixture of s and p waves requires a correlated model.

(ii) *Reaction model.* In this work we use an eikonal model description of the nuclear reaction, improving on the black disk model of Ref. [8].

(iii) *Neutron-core potential.* It is important to include the final-state neutron-core potential in calculating the energy or momentum spectra, as demonstrated in Refs. [11,14]. Reference [9] also included the final-state interaction, using a zero-range neutron-core potential. Our detailed models described here use a realistic finite-range potential in both the initial and final states.

We shall investigate the validity of these as well as other approximations that are often made. Our main interest is the sensitivity of experiments to the properties of the halo nucleus. In a previous work [15] we developed models of the ^{11}Li ground-state wave function with differing amounts of s wave. One of our objectives is to see how well the amount of s wave can be determined by the observables in a breakup reaction. The observables we consider are integrated cross sections for diffraction and one- and two-nucleon removal and the differential cross section for the excitation energy in the $^9\text{Li}+n$ final state when one neutron has been removed.

*Present address: Department für Physik und Astronomy, Universität Basel, CH-4056 Basel, Switzerland.

II. REACTION MODEL

The sudden approximation leads to the eikonal model for nucleus-nucleus interactions. In previous studies, we have applied the model to the nuclear-induced breakup of single-neutron halo nuclei [16]. Here we apply it to the breakup of a two-neutron halo nucleus. The effect of the interaction with the target is to multiply the halo wave function by the profile functions $S(R_i)$ for each particle, where R_i denotes the impact parameter of particle i with respect to a target nucleus. The halo nucleus ^{11}Li has two neutrons and a ^9Li core, requiring two profile functions S_n and S_c associated with neutrons and the core, respectively. There are three integrated cross sections that leave the core intact, namely, the diffractive, the one-neutron stripping, and the two-neutron stripping cross sections. These can be written

$$\sigma_{dif} = \int d^2 R_{cm} \{ \langle [1 - S_c(R_c) S_n(R_1) S_n(R_2)]^2 \rangle - \langle [1 - S_c(R_c) S_n(R_1) S_n(R_2)] \rangle^2 \}, \quad (1a)$$

$$= \int d^2 R_{cm} [\langle S_c^2(R_c) S_n^2(R_1) S_n^2(R_2) \rangle - \langle S_c(R_c) S_n(R_1) S_n(R_2) \rangle^2], \quad (1b)$$

$$\sigma_{1n-st} = 2 \int d^2 R_{cm} \langle S_c^2(R_c) S_n^2(R_2) [1 - S_n^2(R_1)] \rangle, \quad (2)$$

$$\sigma_{2n-st} = \int d^2 R_{cm} \langle S_c^2(R_c) [1 - S_n^2(R_1)] [1 - S_n^2(R_2)] \rangle, \quad (3)$$

where R_{cm} is the impact parameter of the halo nucleus with respect to the target nucleus and $\langle \rangle$ denotes a ground-state expectation value. Our ground-state wave function Ψ_0 is expressed in terms of the relative neutron-core distances r_1 and r_2 . An example of the needed expectation values is the one-neutron stripping integral

$$\langle S_c^2 S_n^2 (1 - S_n^2) \rangle = \int d^3 r_1 d^3 r_2 |\Psi_0(r_1, r_2)|^2 S_c^2(R_c) \times S_n^2(R_c + r_{2\perp}) [1 - S_n^2(R_c + r_{1\perp})]. \quad (4)$$

The integrations are here performed for fixed R_{cm} so R_c depends on the integration variables $R_c = R_{cm} - (r_{1\perp} + r_{2\perp}) / (A_c + 2)$, where A_c is the mass number of the core nucleus.

The six-dimensional integration in Eq. (4) is very time consuming to carry out unless some simplifications are made in the wave function or in the profile functions. We shall consider two simplifying approximations. The first is the *no-recoil limit* in which the impact parameter of the core R_c is assumed to coincide with the impact parameter R_{cm} of the halo nucleus.¹ The core profile function S_c can then be taken outside the expectation value. In addition, the integrations

over r_1 and r_2 become independent in a shell-model representation of Ψ_0 such as Eq. (11). Another simplifying approximation is the *transparent limit*, defined here by setting the factor $S_n^2(R_2)$ equal to one inside the expectation value of Eq. (2), thus neglecting the absorption of the second neutron. These two assumptions yield the cross section

$$\sigma_{1n-st,trans} = 2 \int d^2 R S_c^2(R) \langle 1 - S_n^2(R + r_{1\perp}) \rangle. \quad (5)$$

Note that this cross section is identical to the sum of the one-neutron-stripping cross section and two times the two-neutron-stripping cross section,

$$\sigma_{1n-st,trans} = \sigma_{1n-st} + 2\sigma_{2n-st}. \quad (6)$$

We will see later that the two-neutron-stripping cross section is rather small, so the transparent limit is a good approximation for this cross section.

Of course, much more information about the halo is contained in differential cross sections. The diffractive cross section has three particles in the final state, but that distribution is beyond what we can calculate, requiring three-particle continuum wave functions for many partial waves. The one-neutron stripping leaves two particles in the final state and the differential cross section for that state is amenable to computation. The expression for the momentum distribution associated with the relative motion of the two surviving particles is

$$\frac{d\sigma_{st}}{d^3 k} = 2 \int d^2 R_1 [1 - S_n^2(R_1)] \int d^3 r_{2c} |M(R_1, r_{2c}, k)|^2, \quad (7)$$

where r_{2c} is the center-of-mass coordinate of the remaining neutron-core system with respect to the stripped neutron; the associated impact parameter with respect to the target nucleus is denoted by R_{2c} , $R_{2c} = R_1 + r_{2c\perp}$. The amplitude M is given by

$$M = \int d^3 r_2 \psi_k^*(r_2) S_c(R_c) S_n(R_2) \Psi_0(r_1, r_2). \quad (8)$$

Here $\psi_k(r_2)$ is the continuum wave function of the surviving neutron-core system, normalized to a plane wave at infinity. The coordinates R_c , R_2 , and r_1 are expressed in terms of the integration variables as $R_c = R_{2c} - r_{2\perp} / (A_c + 1)$, $R_2 = R_{2c} + r_{2\perp} A_c / (A_c + 1)$, and $r_1 = -r_{2c} + r_2 / (A_c + 1)$.

The numerical calculation of Eq. (8) is rather difficult because of the form of the ground-state wave function that we apply (see the next section). A major simplification is achieved by adopting the approximation $r_1 = -r_{2c}$ in the ground-state wave function. The amplitude is then given by

$$M' = \int d^3 r_2 \psi_k^*(r_2) S_c(R_c) S_n(R_2) \Psi_0(-r_{2c}, r_2). \quad (9)$$

An even simpler approximation is to ignore the recoil correction in the argument of the core profile function, i.e., set $R_c = R_{2c}$, and use the transparent limit for the second neu-

¹As discussed later on, the no-recoil limit differs from the exact calculation only in the case of diffraction.

TABLE I. Parameter of the different models used in comparing the different cross sections. The first model (*p89*) uses the same potential for *s* and *p* wave, whereas the other two use a deeper potential for the *s* wave (and all other even *L* waves). The strength of the *p*-wave potential is essentially fixed by the position of the $p_{1/2}$ resonance. The lowest two entries give the properties of the uncorrelated pure *s*- and *p*-wave models described in the text.

Model	E_B	V_s (MeV)	a_0 (fm)	$s_{1/2}$ (%)	$p_{1/2}$ (%)	r^2 (fm ²)	$(r_1 - r_2)^2$ (fm ²)	$\left(\frac{r_1 + r_2}{2}\right)^2$ (fm ²)
<i>p89</i>	-0.295	-35.4	+1.7	4.5	89.1	29.4	42.8	18.7
<i>s23</i>	-0.295	-47.5	-5.6	23.1	61.0	37.7	45.9	26.2
<i>s50</i>	-0.292	-51.5	-90.	49.9	33.9	53.8	70.1	36.2
<i>s</i>				100		45.0	90.0	22.5
<i>p</i>					100	27.5	55.0	13.8

tron, i.e., set $S_n(R_2) = 1$. We shall refer to these approximations as the *no-recoil transparent limit*, where the amplitude reduces to

$$M'' = S_c(R_{2c}) \int d^3 r_2 \psi_k^*(r_2) \Psi_0(-r_{2c}, r_2). \quad (10)$$

This approximation is used in Refs. [9,14]. We will discuss the validity of the various approximations in Sec. VI C below.

III. THE THREE-BODY WAVE FUNCTION

In Ref. [15] we constructed several three-body models of ¹¹Li. The models are based on Hamiltonians that all reproduce the empirical neutron-neutron scattering length and all have a binding energy of the three-body system close to the empirical value of 295 ± 35 keV [17]. The single-particle potentials and the density dependence of the neutron-neutron interaction are varied to produce different probabilities of *s* and *p* waves in the different models. Details of the procedure and two of the models are given in Ref. [15]. The wave functions are calculated in the form of single-particle states $u(r)$ and amplitudes α as

$$\Psi_0(\vec{r}_1, \vec{r}_2) = \sum_{l,j} \sum_{n,n'} \alpha_{l j n n'} u_{l j n}(r_1) u_{l j n'}(r_2) [(l s)^j (l s)^j]^0, \quad (11)$$

where \vec{r}_1 and \vec{r}_2 are neutron-core separation vectors. The indices $(l s)^j$ label the single-particle, spin-angle wave functions that are coupled to zero total angular momentum as indicated by the superscript on the bracket. The indices n, n' label the radial quantum numbers of the single-particle basis states. These states are discretized by putting the system into a spherical box of large radius (typically 40 fm).

We will specifically examine the observables for models having 4.5%, 23%, and 50% *s* waves. Their characteristics are given in Table I. The first model *p89* is similar to the one used in Ref. [3]. The other models *s23* and *s50* are constructed with a deeper neutron-core potential for even-parity, single-particle states to increase the *s*-wave component in the ground-state wave function. An important property of the Hamiltonian is the *s*-wave scattering length of neutrons on the core nucleus. Within the constraints of our three-body

model, we can only produce wave functions that are predominantly *s* wave by using neutron-core potentials that produce extremely large *s*-wave scattering lengths. The parameters of the potential for the odd-parity states are fixed by the position of the $p_{1/2}$ resonance, which we assume to be at $E_r = 540$ keV as suggested by measurements [18]. It should be mentioned that other experiments [5,19,20] have extracted different values for the resonance energy. In addition to the *s*-wave probability, these wave functions show significant differences. The single-particle densities of the three models are shown in Fig. 1. It may be seen that the halo is more extended the larger the *s*-wave probability. This is also apparent from the mean-square neutron radii computed in Table I.

The integrated dipole strength for Coulomb breakup is proportional to the mean-square radius of the two-neutron center of mass, given in the last column of Table I. The value obtained with the *p89* wave function is consistent with the experimental Coulomb breakup, but the *s50* value is much too high. Thus we cannot regard that wave function as realistic.

Another important property of the wave function is the correlation between the two neutrons. The integrated dipole strength is proportional to the dineutron-core mean-square radius, which in turn depends on the matrix element of $\vec{r}_1 \cdot \vec{r}_2$, as shown in [3]. In that work it was found that the

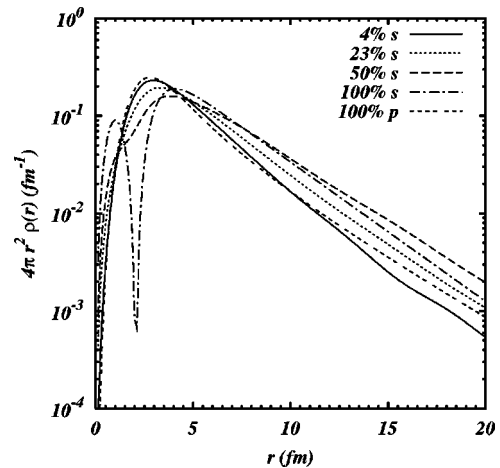


FIG. 1. Single-particle density of halo neutrons in various models of ¹¹Li.

correlation increased the dipole strength by 43%. This enhancement does not depend very much on the model; with the present wave functions it is in the range 30–40 %.

We also constructed s - and p -wave independent-particle models for comparison purposes. In these models, the single-particle potential is adjusted to match the exponential falloff of the single-particle density that is obtained with the three-body model $s23$ mentioned in Table I.

IV. PROFILE FUNCTIONS

We now specify the profile functions S_n and S_c that we use for our cross-section calculations. The neutron profile function S_n in the eikonal approximation is expressed in terms of the density of the target ρ_t and the nucleon-nucleon cross section σ_{nn} as

$$S(b) = \exp\left[-\frac{\sigma_{nn}}{2} \int dz \rho_t(\sqrt{b^2+z^2})\right]. \quad (12)$$

We model the density of the ^{12}C target with the harmonic oscillator fit to the charge density of Ref. [21],

$$\rho(r) = \rho_0[1 + \alpha(r/a)^2]e^{-(r/a)^2}, \quad (13)$$

with $a = 1.687$ fm and $\alpha = 1.067$. The nucleon-nucleon cross section is taken from Ref. [22]; it is 29.2 mb at 280 MeV beam energy.

The reliability of the model can be checked against the nucleon-carbon cross sections. The predicted reaction and elastic cross sections in the eikonal model are

$$\sigma_{re} = \int d^2b [1 - S_n^2(b)], \quad (14)$$

$$\sigma_{el} = \int d^2b [1 - S_n(b)]^2. \quad (15)$$

$$S_c(b) = \exp\left[-\frac{\sigma_{nn}}{2} \int dx dy \int dz \rho_c[\sqrt{(x-b)^2+y^2+z^2}] \int dz' \rho_t(\sqrt{x^2+y^2+z'^2})\right].$$

For the density of ^9Li , we note that it has the same number of neutrons as ^{12}C and we will accordingly take the same parameters for the neutrons. The proton density does not have as many particles in the p shell and we apply the pure harmonic-oscillator model to determine α ($=1/3$) and keep a the same as in ^{12}C . The resulting ^9Li density is parametrized as in Eq. (13) with $a = 1.687$ and $\alpha = 0.726$. This model gives a rms charge radius of 2.28 fm, slightly smaller than the empirical charge radius of ^7Li , which is 2.39 fm. However, the predicted cross section at 800 MeV/nucleon is 840 mb (assuming $\sigma_{nn} = 40$ mb), just 5% larger than the measured cross section of 796 ± 6 mb from Ref. [26]. The cross section at 280 MeV/nucleon has been measured for the

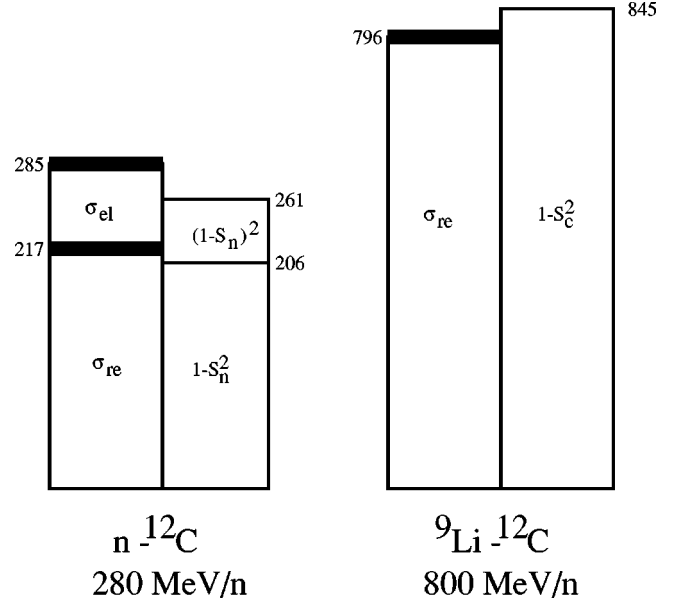


FIG. 2. Cross sections for nucleon- ^{12}C scattering and for ^9Li - ^{12}C scattering. Experimental cross sections are shown on the left with an error band indicated by the thick line. On the right are the cross sections computed with our profile functions.

These are compared with experiment in Fig. 2. The nucleon-carbon reaction cross section is taken from the proton cross section data tabulated in Ref. [23], quoting Ref. [24]. The total cross section for nucleon-carbon scattering is taken from the neutron measurements of Ref. [25]. The experimental elastic cross section is deduced from the difference between total and reaction cross sections. The agreement between our parametrization of S_n and experiment is close enough that we will not attempt to adjust the profile function to make a better fit. In Sec. V we will discuss how the cross sections in halo nuclei depend on the nucleon-target cross sections.

The core-target profile function requires the convolution of both densities

mirror nucleus ^9C by Blank *et al.* [27]. They find a cross section of 812 ± 34 mb to be compared with 796 mb obtained by our model.

For the ^4He core of ^6He we use a three-parameter Fermi density function [21]

$$\rho_c(r) = (1 + wr^2/c^2) / \{1 + \exp[(r-c)/z]\},$$

with $w = 0.517$, $c = 0.964$ fm, and $z = 0.322$ fm. At 800 MeV/nucleon we find a total cross section of 546 mb (486 at 280 MeV/nucleon), again comparable with the experimental result of 503 ± 5 mb [28].

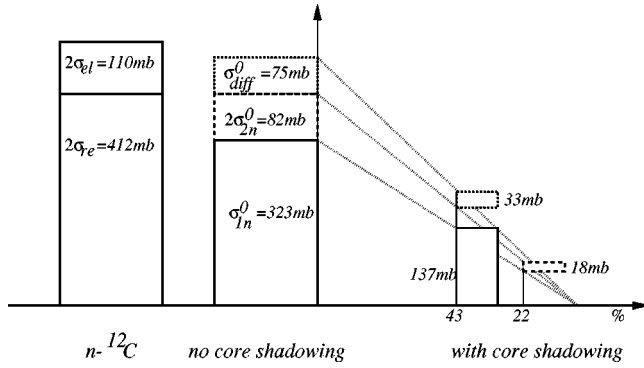


FIG. 3. Breakup reaction cross sections for ^{11}Li - ^{12}C scattering. The left-hand histogram shows twice the n - ^{12}C cross sections as needed in Eqs. (16) and (18). We compare them with the total cross sections without core shadowing (σ^0) in the next histogram. The shadowing reduces the cross section by a factor of ≈ 0.4 for single-neutron stripping and diffraction and by a factor of ≈ 0.2 for two-nucleon stripping, as shown by the diagram on the right-hand side.

V. INTEGRATED CROSS SECTIONS

In this section we examine the integrated cross sections with the aim of understanding the dependence of the cross sections on the interaction and on the properties of the halo. We first discuss some simple bounds and estimates for the various cross sections.

A. Cross-section bounds

Let us first consider the (unrealistic) limit where the core-target interaction is ignored.² For a single-nucleon halo the stripping cross section would then be identical to the reaction cross section σ_{re} between the nucleon and the target. In the case of a two-nucleon halo, the stripping cross section is just doubled. Split into $1n$ - and $2n$ -stripping components, the relation is

$$\sigma_{1n-st}^0 + 2\sigma_{2n-st}^0 = 2\sigma_{re}. \quad (16)$$

The symbol σ^0 is a reminder that the core shadowing is neglected, i.e., the factor S_c is set equal to one. Equation (16) is illustrated in Fig. 3, showing the comparison of the left- and right-hand sides of the equation for the case of ^{11}Li breakup on a ^{12}C target. We used the $s23$ model to evaluate the unshadowed cross section. The relative amounts of $1n$ and $2n$ stripping depend of course on the wave function and details of the interaction; in the case considered here, the $1n$ -stripping cross section is an order of magnitude larger than the $2n$ stripping.

The diffractive cross section is much more difficult to bound or estimate without full calculation of the integrals. In the case of a one-nucleon halo, a bound can be obtained by dropping the second term in the equation analogous to Eq. (1a). The first term is just the elastic nucleon-target cross section, so the bound is $\sigma_{dif}^0 \leq \sigma_{el}$. For ^{11}Be at 800 MeV/

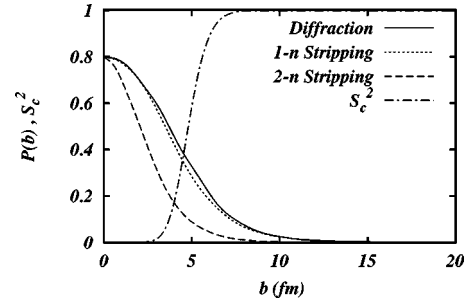


FIG. 4. Impact-parameter dependence of the $1n$ and $2n$ stripping and the diffractive cross sections. Also shown is the square of the profile function of the core-target interaction S_c^2 .

nucleon and using the model of [16] we get $\sigma_{dif}^0 = 68$ mb, which is smaller than the bound $\sigma_{el} = 85$ mb. This shows that the neglected term is not necessarily small. For the two-nucleon diffraction formula (1a) the first term does not reduce to the elastic scattering, so no strict bound can be obtained this way.

Instead, we shall analyze diffractive cross section qualitatively using a gray-disk model for the nucleon-target interaction. Thus we take the nucleon profile function to be of the form $S_n(b) = 1 - t\theta(b_0 - b)$, $0 \leq t \leq 1$. We also need to assume that the two nucleons are uncorrelated in the halo wave function. The diffractive cross section may then be expressed as

$$\sigma_{dif}^0 = 2\sigma_{el} \left[1 - (1 + 2t - t^2/2)a\langle\rho_t\rangle + 2ta^2\langle\rho_t^2\rangle - \frac{t^2}{2}a^3\langle\rho_t^3\rangle \right], \quad (17)$$

where $\langle\rho_t^n\rangle$ is the n th moment of the transverse nucleon density in the halo³ and $a = \pi b_0^2$. The leading term is twice the nucleon-target elastic cross section and the corrections are controlled by the parameter $a\langle\rho_t\rangle$. The coefficient of the first correction is negative, so the first term gives a bound that is valid for large halos and small targets,

$$\sigma_{dif}^0 \leq 2\sigma_{el}. \quad (18)$$

In the case of a ^{12}C target, the experimental elastic and reaction cross sections may be fit with $a = 30$ fm² and $t = 0.5$. The transverse halo density for the ^{11}Li wave functions has the order of magnitude $\langle\rho_t\rangle \approx 1/100$ fm⁻² and the second term makes about a factor of 2 correction; the higher terms are less important. The actual numbers for our model of the ^{11}Li - ^{12}C reaction are shown in Fig. 3. We find $\sigma_{dif}^0 = 75$ mb, reduced from $2\sigma_{el}$ by about a factor 2/3, as expected from the above analysis.

B. Core shadowing

In this section we examine the effect of the core shadowing on the cross sections and use again the model $s23$ for the ground-state wave function. Figure 3 shows on the right-

²This is commonly referred to as the transparent limit, but we have reserved that concept for the transparency of the second neutron in a $1n$ -stripping reaction; cf. Sec. II.

³More precisely, it is the n th moment of an averaged transverse density, the averaging being over the shape of the nucleon profile function.

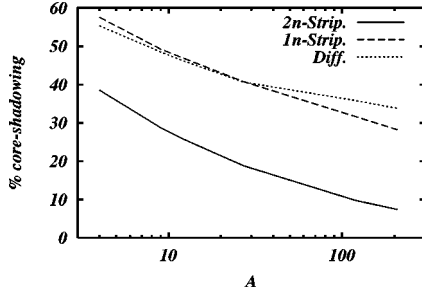


FIG. 5. Shadowing factor as a function of target mass number. Shadowing factors are shown for $2n$ stripping, $1n$ stripping, and diffractive cross sections at an energy of 280 MeV/nucleon.

hand side the shadowing effect of the carbon target in the ^{11}Li breakup reaction. The $1n$ -stripping cross section is reduced to 43% of the unshadowed value σ_{1n-st}^0 . The shadowing factor for the diffractive cross section is very similar (44%) to that for the $1n$ stripping.

The shadowing factor for two-nucleon stripping is much stronger than for the other processes; it reduces the cross section to 20% of the unshadowed value. The difference may be understood qualitatively as follows. The one-nucleon stripping and the diffractive excitation require avoiding an absorptive interaction with at least one of the halo nucleons, favoring moderately large impact parameters. On the other hand, the two-nucleon absorption has no such restriction and would be concentrated entirely at small impact parameters but for the presence of S_c . The different dependences on impact parameter are shown in Fig. 4. Here we see that the $2n$ -stripping probability is more concentrated at small impact parameter than the $1n$ stripping and the diffractive probabilities, which are very similar to each other.

The shadowing factor varies, of course, with target size. This dependence is illustrated in Fig. 5, where the target densities were taken from [21,29]. We see that the shadowing changes by a factor of 2 for both diffraction and $1n$ stripping, going from a ^4He target to a heavy target, and by a factor of 4 for the $2n$ stripping.

C. Wave-function sensitivity

We next consider the sensitivity of the cross sections to properties of the halo wave functions. The various cross sections for different models are given in Table II. For the single-nucleon stripping cross section, the shadowing factor varies depending on how extended the single-particle density is. From Table I we see that the mean-square radius of the halo increases as the s -wave probability increases. Thus we expect less shadowing and a larger cross section for the models with a larger s wave. This is indeed borne out by the

numbers in Table II. For the two-nucleon stripping, the correlation between the neutrons should be important as well, as they must both interact with the target. Indeed, we see from Table II that the two-nucleon cross sections doubles going from an uncorrelated p -wave model to the model with correlations and p -wave dominance. This may be compared with the effect of the correlations on the dipole transition strength, which, as was mentioned in Sec. III, gives only a 30–40 % enhancement.

D. ^6He cross sections

Here we report corresponding cross sections for the breakup of ^6He on a ^{12}C target, using the ^6He wave function from Ref. [15], row 5 of Table II. The cross sections for two different beam energies are shown in Table III. ^6He is more tightly bound than ^{11}Li , so the halo density does not extend out as far. Another difference is that ^6He has a dominant $p_{3/2}$ shell configuration, which allows a stronger spatial correlation; pure $s_{1/2}$ or pure $p_{1/2}$ configurations, on the other hand, have uncorrelated densities. The larger correlation implies that the $2n$ stripping will be relatively stronger. This is indeed seen to be the case in Table III; the $2n$ -stripping cross sections is about a factor of 2 larger for ^6He than for ^{11}Li . Otherwise, the cross sections are about the same as for ^{11}Li . The shadowing factors are similar, due to balancing features of a smaller core and a less extended halo.

VI. FORM OF THE STRIPPING SPECTRUM

In this section we discuss the form of the spectrum in the neutron-core system produced by the $1n$ -stripping reaction. To treat the one-neutron removal from a Borromean nucleus, we simply take the overlap of the initial ground-state wavefunction with the continuum final state of the neutron-core system [cf. Eq. (10)], fixing the position $r_1 = -r_{2c}$ of the stripped neutron. The stripping model assumes that the process is incoherent in r_1 . Thus we consider matrix elements of the form

$$M''(r_1, k) = \int d^3r_2 \psi_k^*(r_2) \Psi_0(r_1, r_2) \quad (19)$$

and a probability distribution of the form

$$|M''(r_1, k)|^2 dn_k.$$

Here $dn_k \sim k^2 dk$ for a differential momentum distribution and $dn_k \sim k dE$ for a differential distribution in excitation energy of the neutron-core system.

Different partial waves of the continuum wave function are incoherent if we integrate over the direction of the decay

TABLE II. Integrated cross sections (mb) with different models of the halo nucleus ^{11}Li .

Channel	Uncorrelated s	Uncorrelated p	p_{89}	s_{23}	s_{50}	Data [6]	Modified data
diffractive	38	26	27	33	40	60 ± 20	94
$1n$ stripping	174	123	121	137	162	170 ± 20	175
$1n$ stripping (transparent)	182	129	134	155	182		
$2n$ stripping	4	3	6	9	10	50 ± 10	11
$2n$ removal	216	152	154	179	212	280 ± 30	280 ± 30

TABLE III. Integrated cross sections (mb) for ${}^6\text{He}$ breakup on ${}^{12}\text{C}$. The experimental number is from Ref. [37].

Channel	240 MeV/nucleon			800 MeV/nucleon		
	with S_c	without S_c		with S_c	without S_c	
diffraction	32.3	64.5	$<2\sigma_{el}=119$	42.7	89.7	$<2\sigma_{el}=168$
1n stripping	136	286		144	319	
1n stripping (transparent)	170	409	$\approx 2\sigma_{re}=414$	184	488	$\approx 2\sigma_{re}=493$
2n stripping	16.7	61.6		19.8	84.1	
σ_{-2n}	185			206		$\sigma_{\text{expt}}=189\pm 14$

distribution. At low energies the s and p waves will be most important. In principle, the stripping distributions are sufficiently dissimilar that one can extract the ratio of probabilities from experiment. The important question then arises how this number reflects the probability in the wave function, which is the ultimate object of the measurement. A comparison of the two probabilities for various models is shown in Fig. 6. The amount of s wave in the final-state stripping distribution is systematically larger than in the wave function of the initial state. This is to be expected and is due to the larger extension of the s wave and consequent decrease in the shadowing. This amounts to about 10% in the extracted probability.

Next we want to discuss analytic forms for the shape of the spectrum in the neutron-core final state produced by the 1n-stripping reaction. The standard parametrization of a peaked distribution by the Breit-Wigner function is not justified at energies close to zero or for the overlaps with extended wave functions. We shall propose parametrizations that take into account the threshold behavior and the halo character of the initial state. Throughout this section we make use of the no-recoil transparent limit defined in Eq. (10).

A. s -wave distribution

The s -wave distribution can be described analytically in the limit where the wave functions are dominated by their asymptotic behavior.⁴ The continuum s wave is then given by

$$\psi_k(r) = \frac{\sin(kr + \delta)}{kr}.$$

Here δ is the s -wave phase shift; the scattering length is the linear coefficient in the expansion

$$\delta = -ak + O(k^3).$$

The two-particle initial-state wave function has no exact analytic limit, but the general exponential falloff at large distances suggests the approximation

$$\Psi_0(r_1, r_2) \approx f(r_1) \frac{e^{-\alpha r_2}}{r_2}.$$

Then the integral in Eq. (19) can be carried out to give

$$M''(r_1, k) \approx f(r_1) \frac{\cos(ka) - \alpha/k \sin(ka)}{k^2 + \alpha^2}$$

and therefore the cross section for the s wave is given by

$$\frac{d\sigma}{dE} \sim |M''|^2 k \sim k \left[\frac{1}{\alpha^2 + k^2} \right]^2 \left[\cos(ka) - \frac{\alpha}{k} \sin(ka) \right]^2. \quad (20)$$

This depends on the initial-state potential through the falloff parameter α and on the final-state potential through the scattering length a . If the two potentials are the same, then the orthogonality of initial and final states requires the matrix element to vanish. This comes about in Eq. (20) to leading order in k by the well-known relation between the binding energy and scattering length [31].

The s -wave energy distribution for ${}^{11}\text{Li}$ is shown in Fig. 7. Here we have fitted both parameters α and a to give the best agreement with the calculated curve, which was obtained in the no-recoil transparent limit [cf. Eq. (10)] using the model $s23$. In a one-nucleon halo α is related to the binding energy by $\alpha \approx \sqrt{2mE_B}$. Our fit has $\alpha = 24.5 \text{ MeV}/c$. The corresponding binding energy is 0.32 MeV, almost equal to the binding energy of the independent-particle model. Also our fitted value $a = -4.7 \text{ fm}$ is very close to the scattering length of the model, -5.6 fm .

The distribution in Fig. 7 peaks at very low energies; the peak position is close to the momentum $k = \alpha/2$ for a fairly

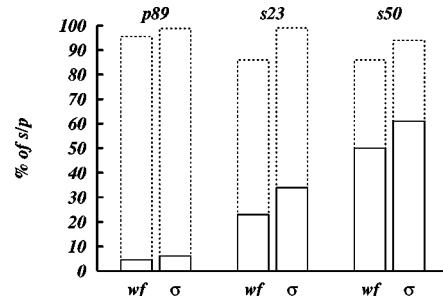


FIG. 6. Percentage of s and p waves in the various models, comparing the probabilities in the wave functions (wf) to the probabilities in the neutron-core final states (σ).

⁴The result (20) was first applied to the photodisintegration of the deuteron at low energy, where it gives an excellent approximation [30].

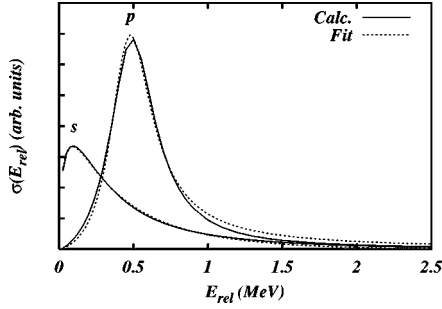


FIG. 7. The ^{11}Li $1n$ -stripping energy distributions in the no-recoil transparent limit (solid curves) are compared to fits obtained from Eq. (20) and Eqs. (21) and (22) (dashed curves). Shown are the s - and p -wave components of the s_{23} wave function.

wide range of scattering lengths a between $-1/\alpha$ and $1/\alpha$. This corresponds to an energy peak E_{peak} at

$$E_{peak} = E_B/4.$$

With our theoretical fit, $E_{peak} \approx 0.08$ MeV. It should also be mentioned that for models with very large scattering lengths, such as the s_{50} model, the scattering length sets the momentum scale and the predicted peak is even lower in energy.

The corresponding s -wave distribution for ^6He is shown in Fig. 8. Here the best-fit scattering length parameter is $a = 1.6$ fm, to be compared with the actual scattering length of $a = 2.4$ fm associated with the ^5He potential. The best fit value of α is $\alpha = 55$ MeV/ c ; this may be compared with the binding energy estimate $\sqrt{2mE_B} = 43$ MeV/ c .

B. p -wave distribution

For the p -wave, measurements of the $^{11}\text{B}(^7\text{Li}, ^8\text{B})^{10}\text{Li}$ reaction have suggested the existence of a resonance at about 540 keV [18]. In our recent study of the ^{11}Li wave function we used this data to fix the p -wave potential for the neutron-core system. In this section we wish to establish a simple function to represent the distributions that we calculate. After trying different functional forms, we found that one could get acceptable fits with the Breit-Wigner resonance form but using a two-parameter energy-dependent width. The threshold behavior of a p -wave resonance requires a width depending on energy as $\Gamma \sim E^{3/2}$. However, the width cannot continue to grow as the $3/2$ power at energies above the

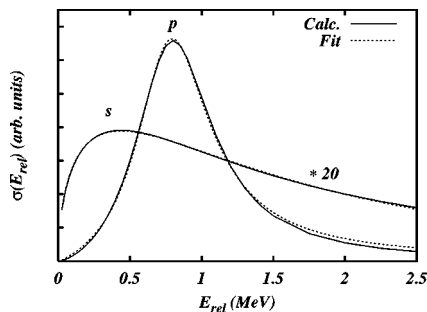


FIG. 8. The ^6He $1n$ -stripping energy distributions calculated in the no-recoil transparent limit (solid curves) are compared to fits obtained from Eq. (20) and Eqs. (21) and (22) (dashed curves). The s -wave components have been scaled by a factor of 20.

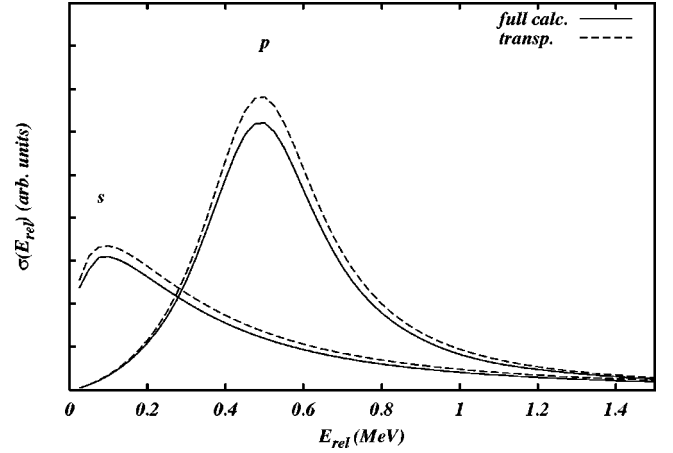


FIG. 9. Comparison of the s - and p -wave distributions for transparent limit with the complete calculation, including shadowing of the spectator neutron, for the s_{23} model.

resonance. We shall account for this by using the form of the p -wave width obtained in potential scattering [32]

$$\Gamma = E^{3/2} \frac{g_1}{1 + g_2 E}. \quad (21)$$

The Breit-Wigner function for the decay of a resonance is then given by

$$\frac{d\sigma}{dE} = A \frac{\Gamma}{(E - E_R)^2 + \Gamma^2/4}. \quad (22)$$

There are four parameters here, namely, the resonance energy E_R , two width parameters g_1 and g_2 , and the overall strength A . One might think that g_1 and g_2 could be determined by the radius of the potential forming the resonance, but because the initial state is a halo the length scales are larger than the nuclear radius. We shall treat them as adjustable parameters. Figure 7 shows a fit with parameter values $g_1 = 2.74$ MeV $^{-1/2}$ and $g_2 = 3.3$ MeV $^{-1}$. When we make an unconstrained fit, the parameter g_2 becomes large, showing that the function Γ is close to the $E^{1/2}$ dependence, except at extremely low energies.

In Fig. 8 we show a similar comparison for ^6He stripping. In this case, the peak of the p -wave distribution is located at 0.83 MeV, which corresponds quite well to the resonance energy of the $p_{3/2}$ scattering state (0.89 MeV). Nevertheless, the best fit again favors large values of g_2 , indicating that the $3/2$ power law for the width is only valid very close to the threshold.

C. Simplifying approximations

Since the full calculations with Eqs. (7) and (9) are quite time consuming, it is of interest to know how accurate simplifying approximations are. We examine the transparent limit, the no-recoil approximation, and the relation between the stripping probability and wave function probability here.

1. Transparent limit

The energy distribution in the no-recoil transparent limit is compared to the full calculation in Fig. 9 for ^{11}Li strip-

ping, using the s_{23} ground-state wave function. We see that the effect of the neutron shadowing is to reduce the cross section without affecting the energy distribution. Thus we can use the transparent limit with confidence in describing these distributions.

2. No-recoil approximation

The no-recoil approximation is exact for integrated stripping cross sections, but it can in principle affect the differential stripping and both differential and integrated diffractive cross sections. For the integrated diffractive cross section in ^{11}Li , we find that the effect of the recoil is to reduce the cross section by 20%. Since the corrections are expected to scale as $1/A$, one should not ignore them for nuclei lighter than ^{11}Li .

In our calculations of stripping distributions, we have included the main recoil effect as described in Sec. II, Eq. (9). However, there is a residual recoil effect associated with the position of the stripped neutron; cf. Eq. (8). We calculated a spectrum from Eq. (8) in the independent p -wave model, at fixed impact parameter. The approximation (9) was found to be very accurate, with the deviation in the peak of the order of 1/2% and the maximum deviation smaller than 3%.

VII. COMPARISON WITH EXPERIMENT

A. Integrated cross sections

In Table II we compare the integrated cross sections with the experimental data of Ref. [6], Table 3. The yields of events having zero, one, or two neutrons in coincidence with the ^9Li fragment give, respectively, the cross sections labeled $2n$ stripping, $1n$ stripping, and diffraction. The first thing to note in the comparison with theory is that the total two-neutron removal cross section measured, 280 mb, is much larger than the eikonal model predicts. There are also data on the two-neutron removal cross section at 800 MeV/nucleon [33]. Applying the eikonal model.⁵ at this energy gives a cross section of 187 mb (s_{23} wave function), only 15% lower than the experimental value of 220 ± 10 mb. At the lower energy the s_{23} model gives 179 mb. This is close to the theoretical value at the higher energy, which is certainly to be expected in view of the mild change in the nucleon-nucleon cross section between the two energies. The direction of the change in both the nucleon-nucleon and the eikonal removal cross section is a decrease at the lower energy. In contrast, the experimental value is larger at the lower energy. The theoretical two-neutron removal cross section behaves the same way in the case of ^6He , as may be seen in the bottom row of Table III. Here also there is fair agreement with the experimental value at the higher energy.

Let us now turn to the individual components. The diffractive and $1n$ -stripping cross sections are within experimental error of the most extreme wave function s_{50} , but the $2n$ -stripping cross section far exceeds any of the models. In principle, additional contributions to the cross section could come from processes outside the scope of the eikonal model.

The flux that is absorbed in the eikonal can reappear, e.g., by multistep or rearrangement processes. This might first show up in cross sections that are very small in the eikonal model, such as the $2n$ stripping. Another possibility is that the direct connection between the different components of the observed cross section and the three reaction mechanisms has been distorted by the experimental acceptance. To correct for this distortion involves some uncertainty. We shall anyway make a simple estimate that shows that it is possible to reduce the large discrepancy between the calculated and the measured $2n$ -stripping cross sections.

The experimental acceptance of neutrons was limited to transverse momenta up to 95 MeV/ c and it was estimated that only about 80% of the diffracted neutrons would be detected [6]. By extrapolating the measured transverse momentum distribution of neutrons shown in Fig. 3 of Ref. [34] to large momenta, one also finds that about 80% of all neutrons have transverse momenta less than the 95 MeV/ c acceptance. The detection efficiency for spectator neutrons (produced when the second neutron is either stripped or diffracted) may be higher, but let us just assume that it is also 80%. The relations between the measured cross sections σ' and the full-acceptance cross sections σ are then $\sigma'_{dif} = (0.8)^2 \sigma_{dif}$, $\sigma'_{1n-st} = (0.8)\sigma_{1n-st} + 2(0.8)(0.2)\sigma_{dif}$, and $\sigma'_{2n-st} = \sigma_{2n-st} + (0.2)\sigma_{1n-st} + (0.2)^2 \sigma_{dif}$. Solving these equations for the full-acceptance cross sections gives the values shown in the last column of Table II labeled ‘‘Modified data.’’

As may be seen from the table, adding the detector acceptance correction explains the small $2n$ -stripping cross section, but only at the expense of greater disagreement with theory for the other two cross sections. Thus, for the diffractive cross section, we obtain less than half the experimental value. We believe that it is not possible to explain this discrepancy within the framework of the eikonal model. Recall that the unshadowed diffractive cross section has a quasi-bound $\sigma_{dif}^0 < 2\sigma_{el} \approx 120$ mb valid for very extended halos and the actually computed cross section is reduced from this by two factors of 2. The first reduction, seen in Eq. (17), is associated with the fact that the nucleon-target profile function blocks a significant fraction of the halo density. The second factor is the shadowing of the halo density by the core-target profile function. This shadowing is unavoidable and reduces the diffractive cross section by an additional factor of 2.

For the $1n$ -stripping cross section with an assumed 20% acceptance correction, the eikonal model can explain the data, but only if the s -wave component is large. However, we believe that the model that comes closest, s_{50} , is unrealistic on other grounds.

B. Relative energy spectrum

In the analysis made in [6] two Breit-Wigner resonances were fitted, at 0.21 ± 0.05 and 0.62 ± 0.10 MeV, and the relative amounts of s and p waves in the wave function were extracted. Let us see how this compares with our analysis with the calculated distributions. As discussed in Sec. VI, we find a peak for the final s wave at a much lower energy than the experimental spectrum shows. However, the finite angular and energy resolution of the experimental detectors will

⁵We note that Ref. [7] obtained 241 mb, i.e., 10% higher than experiment, in their eikonal model.

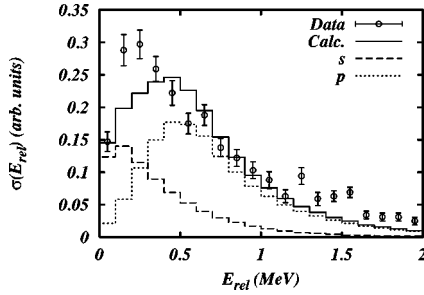


FIG. 10. Energy distribution of the s_{23} wave function. The histogram is the calculated result including the experimental resolution. The solid line is the result for all partial waves. Also shown are the s - and p -wave components (dashed and dotted lines). The data points are from Ref. [6].

inevitably smear out the distribution of the extracted relative momentum or energy, shifting the apparent peak to higher energy. This should be taken into account in comparing our spectrum with the experiments.

The authors of Ref. [6] give a table of transverse momentum and longitudinal velocity resolution widths and we have folded these widths with the theoretical spectra to compare with experiment.⁶ The folding is done by Monte Carlo sampling. We generate events, sampling the theoretical distribution of E in the center-of-mass system of the neutron-core system and assuming that the angular distribution is isotropic there. We add a Gaussian-distributed center-of-mass momentum. As we do not have any cuts in our simulation, this center-of-mass momentum is not important. We transform then from the projectile frame to the laboratory frame, determining the transverse momentum as well as the Lorentz β in the laboratory frame. To these we add random errors from a Gaussian distribution with a full width at half maximum given by Table 2 in [6]. The relative energy [Eq. (3.2) of [6]] is reconstructed using these values, which are then binned into the same energy intervals as the experiment.

Figure 10 shows the result of this procedure for the s_{23} model. The experimental resolution increases the position of the s -wave peak from 0.08 MeV to 0.15 MeV, which is close to the value 0.21 ± 0.05 deduced by the Breit-Wigner fit. However, with our shapes for the individual components, the measured peak at 0.21 MeV is a combined effect of both s and p waves. The individual spectra are strongly overlapping and require a realistic model of the shapes to separate them with confidence.

One of our main goals is to find out what we can conclude from this spectrum about the s -wave contribution in the ground state and also about the position of the p -wave resonance. To investigate this, we tried to make a best fit of a theoretical spectrum to the data. The theoretical spectrum is convoluted with a momentum resolution function as described earlier to generate a simulated experimental spectrum. We then make a χ^2 minimization with respect to the parameters in the theory. The first fit was done in the framework of our Hamiltonian, allowing the s -wave potential and

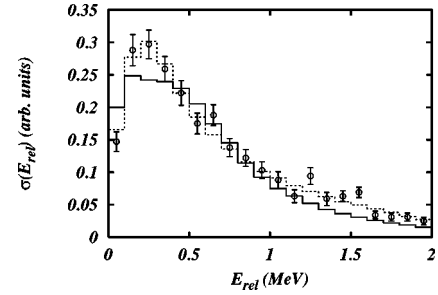


FIG. 11. Fits of the energy distribution to the data of Ref. [6], including the experimental resolution. The solid line is obtained from the best-fit Hamiltonian model. The dotted line is the result from fitting Eqs. (20) and (22) with $a = -1$ fm, $E_R = 0.25$ MeV, and an s/p ratio corresponding to 66% s wave.

the interior interaction to vary. The best fit, shown as a solid line in Fig. 11, is for a model with 35% s wave with a range 25–40 % giving similar quality fits. We see that the fit is not entirely satisfactory, however, being flatter at the lowest energies than the first two data points require.

The second fit procedure was using the parametrizations (20) and (22), allowing E_R , a , and the s/p ratio to vary. The p -wave width parameters were kept fixed to the values in Sec. VI B. This fit is better, as is to be expected with more parameters. In particular, the threshold region is well described. The resonance energy E_R came out lower than we assumed earlier; a good fit could be made with E_R in the range 0.25–0.35 MeV. This corresponds more to the value obtained by other experiments [19,20] than to the one we used [18] in setting up our Hamiltonian. The fitted scattering length comes out rather small and attractive, in the range of -1 to -2.5 fm. With a lower p -wave resonance energy and a weakly attractive s wave, one might expect that the p component would be dominant, but this is not the case. The fit gives an s probability of 66% with good fits in the range 60–70 %. It will be a challenge that we must leave for the future to construct a realistic Hamiltonian that would reproduce this behavior.

C. Transverse momentum distribution

In order to test our final-state spectrum, we also make comparisons to a measurement of the transverse momentum distribution of neutrons. Such a measurement has recently been performed at the same energy [34]. In our analysis we assume that the momentum distribution of the neutrons is isotropic and identical to the relative momentum distribution of the neutron and the core fragment. The relative energy spectrum can then be transformed into a transverse momentum distribution

$$\frac{d\sigma}{d^2k_{\perp}} = \int_0^{\infty} dk_l \frac{1}{2\pi mk} \frac{d\sigma}{dE}.$$

In Fig. 12 we compare the result of our “best” Hamiltonian model with the experimental result. In this figure we made no attempt to include the experimental resolution in the theory curve. The agreement between theory and experiment is similar to the model fit in Fig. 11. The main part of the cross section comes in the correct range of momentum, but

⁶Reference [6] also quotes an energy resolution function ($\Delta E \sim E^{0.75}$), but this does not go to a finite value near $E=0$, so we prefer to construct the resolution as described.

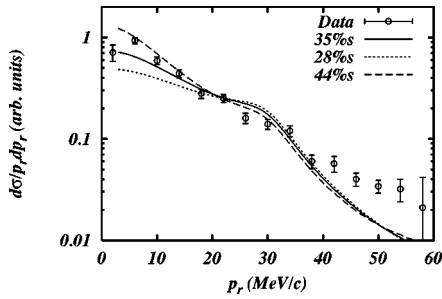


FIG. 12. Transverse momentum distribution including all partial waves of the best-fit model. Shown are the results with 28%, 35%, and 44% s -wave component in the final state, corresponding to a ^{11}Li ground-state component between 20% and 40%. The data points are from Ref. [34].

the curve does not describe the very high and very low momenta well. This disagreement may be partly due to diffractive effects [6], which have been ignored here.

VIII. CONCLUSIONS AND OUTLOOK

In this paper we applied the eikonal theory to nuclear breakup of Borromean nuclei, with the object of developing a quantitative tool for interpreting reaction cross sections. Because the full theory is quite demanding from a numerical point of view, we examined the approximations that are commonly made. In particular, the theory simplifies if one neglects correlations in the ground-state wave function, the final-state interaction, the distortion effects of the profile functions on unstripped particles, or the difference between vectors referred to various center-of-mass systems.

The easiest cross section to interpret is the one-particle stripping, which leaves a particle and the core in a final state of low excitation energy. The integrated one-particle stripping cross section can be calculated with rather rough approximations. The correlations in the ground state play no role except to determine occupation probabilities for the shell orbitals. In the differential cross section, the distributions of s and p waves are quite distinct, allowing the occupation probabilities of the ^{11}Li halo orbitals to be extracted with 10–20 % accuracy. Many of the simplifying approximations can be used here without significant error. The distortion introduced by the profile functions has practically no effect on the shape of the distributions and a moderate effect on the extracted relative probabilities. However, it is important to include the final-state interaction in the particle-plus-core system [14]. We proposed parametrizations of the s - and p -wave distributions that take both the initial halo character and the final-state interaction into account. The s -wave distribution, given by Eq. (20), is derived from the asymptotic wave functions. The p -wave distribution, given by Eqs. (21) and (22), is in the form of a Breit-Wigner function with an energy-dependent width. The width varies with energy as $\Gamma \sim E^{3/2}$ at threshold, but the threshold region is very narrow due to the extended initial wave function. At higher energies the width grows more like $\Gamma \sim E^{1/2}$, which is the characteristic behavior in the absence of a barrier.

The other two integrated cross sections are more sensitive to the correlations in the wave function. The two-particle stripping cross section is sensitive to the pairing correlation,

nearly doubling when pairing is included. If the two-nucleon stripping could be measured well, it could be used to study this aspect of the wave function. The other integrated cross section, the diffractive cross section, is not only sensitive to the eikonal distortions, but we found that it changes significantly if the recoil correlation is included in the wave function. The differential diffractive cross section is presently beyond our computational powers.

As a specific example, we have applied the eikonal analysis to the data of Ref. [6]. The total two-neutron removal cross section is larger than our calculation and also larger than the experimental value at a higher energy (800 MeV/nucleon). This is surprising because the difference in nucleon-nucleon cross sections at the two energies demands the opposite trend in the eikonal model. Our calculated one-neutron stripping and diffractive cross sections are only 75% and 50% of the measured values, respectively. The experimental diffractive cross section is nearly high enough to be in conflict with the bound given by Eq. (18).

In analyzing the differential cross section, we found some general features that should be useful in future studies. First of all, the approximations of no recoil and the transparent limit give a rather good account of the one-particle stripping distribution, justifying these approximations. The s -wave distribution can be fit very well by a simple formula based on the asymptotic wave functions (20), which is quite different from the Breit-Wigner distribution. The p -wave cross section can be reproduced by a Breit-Wigner distribution using an energy-dependent width.

In comparing the stripping distribution with experiment, we found that both s and p waves are needed to fit the data of Ref. [6]. Our s distribution peaks at a very low energy and the experiment does not show as much of a threshold enhancement as we predict. In our least constrained fit, we obtained a p -wave resonance near 0.3 MeV, lower than the measurement of Ref. [18]. The experimental peak is at 0.2 MeV and is most likely due to the combined effect of s and p waves. Our analysis with the Hamiltonian models gives an s -wave component of between 30% and 50% in the cross section, which corresponds to an s -wave probability in ^{11}Li between about 20% and 40%. Our least constrained fit has a high s -wave probability, 60–70 %. A number of other experimental [5,18,34,6,35] and theoretical studies [10,36] have extracted s -wave probabilities of about 50%. An even larger value is apparently obtained by Garrido, Fedorov, and Jensen [14], who report a p -wave probability of 26%. In conclusion, the eikonal theory has considerable promise for interpreting the distributions and cross sections in nuclear breakup, but it has not yet proved to be a quantitative tool for the reaction we studied.

ACKNOWLEDGMENTS

We would like to thank W. Dostal and H. Emling for discussions and for providing unpublished data from the experiment in Ref. [6]. This work was supported by the Swiss National Science Foundation, the Freiwillige Akademische Gesellschaft of the University of Basel, the Deutsche Forschungsgemeinschaft, and the U.S. Department of Energy, Nuclear Physics Division, under Contract Nos. W-31-109-ENG and DE-FG-06-90ER-40561.

- [1] D. Sackett *et al.*, Phys. Rev. C **48**, 118 (1993).
[2] S. Shimoura *et al.*, Phys. Lett. B **348**, 29 (1995).
[3] G. F. Bertsch and H. Esbensen, Ann. Phys. (N.Y.) **209**, 327 (1991).
[4] H. Esbensen, G. F. Bertsch, and K. Ieki, Phys. Rev. C **48**, 326 (1993).
[5] R. A. Kryger *et al.*, Phys. Rev. C **47**, 2439 (1993).
[6] M. Zinser *et al.*, Nucl. Phys. **A619**, 151 (1997).
[7] Y. Ogawa, K. Yabana, and Y. Suzuki, Nucl. Phys. **A543**, 722 (1992).
[8] F. Barranco, E. Vigezzi, and R. A. Broglia, Phys. Lett. B **319**, 387 (1993).
[9] F. Barranco, E. Vigezzi, and R. A. Broglia, Z. Phys. A **356**, 45 (1996).
[10] I. J. Thompson and M. V. Zhukov, Phys. Rev. C **49**, 1904 (1994).
[11] A. A. Korshennikov and T. Kobayashi, Nucl. Phys. **A567**, 97 (1994).
[12] Y. Ogawa, Y. Suzuki, and K. Yabana, Nucl. Phys. **A571**, 784 (1994).
[13] P. Banerjee and R. Shyam, Phys. Lett. B **349**, 421 (1995).
[14] E. Garrido, D. V. Fedorov, and A. S. Jensen, Phys. Rev. C **53**, 3159 (1996).
[15] H. Esbensen, K. Hencken, and G. F. Bertsch, Phys. Rev. C **56**, 3054 (1997).
[16] K. Hencken, G. F. Bertsch, and H. Esbensen, Phys. Rev. C **54**, 3043 (1996).
[17] B. M. Young *et al.*, Phys. Rev. Lett. **71**, 4124 (1993).
[18] B. M. Young *et al.*, Phys. Rev. C **49**, 279 (1994).
[19] H. Bohlen *et al.*, Z. Phys. A **344**, 381 (1993).
[20] H. Bohlen *et al.*, Nucl. Phys. **A616**, 254 (1997).
[21] C. DeJager, H. DeVries, and C. DeVries, At. Data Nucl. Data Tables **17**, 479 (1974).
[22] K. Charagi and S. K. Gupta, Phys. Rev. C **41**, 1610 (1990).
[23] W. Bauhoff, At. Data Nucl. Data Tables **35**, 429 (1986).
[24] P. U. Renberg *et al.*, Nucl. Phys. **A183**, 81 (1972).
[25] J. Franz *et al.*, Nucl. Phys. **A490**, 667 (1988).
[26] I. Tanihata *et al.*, Phys. Rev. Lett. **55**, 2676 (1985).
[27] B. Blank *et al.*, Nucl. Phys. **A624**, 242 (1997).
[28] I. Tanihata *et al.*, Phys. Lett. **160B**, 380 (1985).
[29] H. DeVries, C. DeJager, and C. DeVries, At. Data Nucl. Data Tables **36**, 495 (1987).
[30] S. deBenedetti, *Nuclear Interactions* (Wiley, New York, 1964), p. 274.
[31] L. Elton, *Introductory Nuclear Theory* (Pitman, London, 1959), Eq. (3.75).
[32] A. Bohr and B. Mottelson, *Nuclear Structure* (Benjamin, New York, 1969), Vol. I, Eqs. (3F-38–44).
[33] T. Kobayashi *et al.*, Phys. Lett. B **232**, 51 (1989).
[34] M. Zinser *et al.*, Phys. Rev. Lett. **75**, 1719 (1996).
[35] N. Aoi *et al.*, Nucl. Phys. **A616**, 181c (1997).
[36] N. Vinh Mau and J. C. Pacheco, Nucl. Phys. **A607**, 163 (1996).
[37] I. Tanihata, D. Hirata, T. Kobayashi, S. Shimoura, K. Sugimoto, and H. Toki, Phys. Lett. B **289**, 261 (1992).